BOLETIN DE LA SOCIEDAD ESPAÑOLA DE
Cerámica y Vidrio
A R T I C U L O

Development and control of microstructures in directionally solidified $REBa_2Cu_3O_7$ (RE=Y,Nd) superconductors

F. SANDIUMENGE
Institut de Ciència de Materials de Barcelona, Consell Superior d'Investigacions Científiques. Campus de la Universitat Autònoma de Barcelona, 08193 Bellaterra, Catalunya, Spain

Directionally solidified $REBa_2Cu_3O_7$ (RE=Nd,Y) superconductors display a complex microstructure which is generated during the solidification and annealing processes. The various defects influence the superconducting properties in different ways. The present article briefly reviews the characteristics of the different defect structures and evolution in connection with their effect on the critical currents. In this work, the defects are classified into strong pinning centres and currents limiting defects. Dislocation problems are addressed separately, emphasising on the generation of stacking faults, oxygenation effects and plastic deformation processing.

Key words: Ceramic superconductors, microstructure, flux pinning centres, current limiting defects, processing.

Desarrollo y control de microstructuras en superconductores $REBa_2Cu_3O_7$ (RE=Y,Nd) solidificados direccionalmente

Los superconductores de composición $REBa_2Cu_3O_7$ (RE=Nd,Y) preparados mediante solidificación direccional presentan una microestructura compleja que se desarrolla durante las etapas de solidificación y tratamientos de recocido posteriores. Los diversos defectos influyen sobre las propiedades superconductoras de manera desigual. El presente artículo revisa brevemente las características de las diferentes estructuras de defectos y su evolución conectando con su efecto sobre las corrientes críticas. Los defectos, en este trabajo, se clasifican en centros fuertes de anclaje de flujo y defectos que limitan la corriente. Los problemas asociados con las dislocaciones se tratan separadamente, poniendo el énfasis en la generación de defectos de apilamiento, problemas de oxigenación y deformación plástica.

Palabras clave: Superconductores cerámicos, microestructura, centros de anclaje de flujo, defectos limitadores de corriente, procesado.

1. INTRODUCTION

Demands of high critical currents in $REBa_2Cu_3O_7$ (RE=Nd,Y) RE123 superconductor ceramics ($J_c>10^4$ A/cm^2) in a magnetic field and near T_c raise several microstructural-processing problems derived from the particular physics and complex chemistry and microstructure of high temperature superconductors. The first challenge was to develop a processing route for the preparation of large single domain tiles, thus avoiding weak link behaviour associated with growth induced grain boundaries (see Ref. 1 for a review on melt processing of ceramic superconductors). This initial problem was overcome by directional solidification through the peritectic temperature of RE123 compounds. These materials decompose peritectically at temperatures around ~1100°C into a liquid phase and solid Y_2BaCuO_5 (Y211) or $Nd_4Ba_2Cu_2O_{10}$ (Nd422) particles. During solidification an important fraction of non-reacted particles are trapped by the growth front. Interestingly, the interface between such non-superconducting inclusions (size around 2 to 15 μm) was found to constitute a strong pinning centre. In Y123, solidification routes incorporating suitable dopands acting as nucleation centres for the non-reacted or added Y211 particles, such as CeO_2 (2), have allowed to decrease their size down to the sub micrometer range thus increasing the total interface area and J_c up to 10^5 A/cm^2 at 77K in self field (2).

Unfortunately, state of the art bulk ceramics still display J_c values about a factor ten below those achieved in optimised thin films or single crystals. New challenges are on the one hand, identification and control of current limiting defects, and on the other hand, the introduction of structural defects suitable to pin the flux lines in order to decrease thermally activated flux flow when the magnetic field is oriented perpendicular to the CuO_2 superconducting layers. However, if the superconducting behaviour is markedly two-dimensional (2D), microstructural properties also present a strong 2D nature, being very difficult to create correlated defects along the c-axis as, e.g., dislocation lines, by conventional processing. More sophisticated techniques, like heavy ion irradiation (3) which provide strong correlated pinning sites along ion tracks, or the use of high energy protons to fission Bi in Bi-based ceramic superconductors (4), have yielded excellent results. However such methods suffer from the problem of easy translation to the industrial scale. Therefore, from a practical point of view, chemical paths for J_c enhancement seem the more feasible. The last relevant achievement refers to MgO nano-rods in a Bi-based superconductor (5).

In fact, RE123 have a complex microstructure with a wide spectrum of structural defects which affect the superconducting properties in various ways (see Ref. 6 for a review) difficulting the correlation of individual defects with bulk electromagnetic measures. Some selected topics are reviewed here, with emphasis on nature of the defects and their evolution.

2. SUPERCONDUCTOR-NON SUPERCONDUCTOR INTERFACES

The most prominent defect in melt textured RE123 composites is the superconductor-non superconductor interface given by non reacted inclusions dispersed within the single domain matrix. A high concentration (around 20 to 30 wt%) of submicrometric non-reacted inclusions is beneficial for the mechanical and superconducting properties of the composite. First, they act as effective stoppers against microcrack propagation (7), and therefore enhance the mechanical toughness of the ceramic. Secondly, in Y123 it has been experimentally verified that J_c scales with the total interface area (8,9).

The size of Y211 particles in the melt can be modified by Ostwald-ripening (10). Soaking experiments performed on relative short periods of a few tens of hours have indeed revealed coarsening behaviour, which in directional solidification translates into Y211 size variations in the samples (11). However, particle coarsening may be inhibited by small concentrations of additives such as Pt (12) or CeO_2 (2,13,14). For instance, no significative inclusion size variations were detected within the time scale (~100 h) of the solidification of long length composites (up to 12 cm) (7). Therefore, the coarsening effects on the size distribution of Y211 particles in long ceramic bars may be limited by the use of suitable additives.

Since the interface pinning strength is proportional to the gradient of the superconducting order parameter at the interface (8), it will be highly sensitive to lattice defects which should smooth out the variation of the superconducting order parameter. In agreement with such considerations, HRTEM images show atomically sharp Y123-Y211 interfaces (7,15).

On the other hand, comparison of the self-field $J_c(T)$ dependencies in Nd123 and Y123 show some distinctive features which point to a reduced efficiency of the interface pinning mechanism in melt processed Nd123 (16). Interestingly, preliminary HRTEM studies of Nd123-Nd422 interfaces point to the occurrence of different interfacial defects which could be at the origin of the observed characteristics of the thermal dependence of J_c in Nd123. Preliminary results are summarised below.

Fig. 1 shows a HRTEM image of an edge on Nd123-Nd422 interface where the Nd123 is slightly deviated (by ~1°) from the $[010]_{Nd123}$ zone axis and the Nd422 particle is viewed along $[0\bar{1}1]_{Nd422}$. The interface plane in this area corresponds to the $(100)_{Nd422}$ plane. The $(001)_{Nd123}$ planes are inclined by α=64° to the interface. For this orientation it can be observed that the prominent bright matrix planes, spaced by one c-axis length, meet the interface approximately at every three $(011)_{Nd22}$ lattice spacings, i.e. $3d(011)_{Nd422}\sin\alpha \sim d(001)_{Nd123}$. Therefore, both crystals are oriented such that some degree of lattice matching exists at the interface. It can be observed that the interface contains a slab of highly strained material about 11 Å thick which probably results from strain relaxation at the interface (16). Other observations strongly suggest that the local structure at the Nd123-Nd422 interfaces can also be affected by local surface dissolution of the Nd422 particles (17). Fig. 2 shows an HRTEM image of a Nd123-Nd422 interface with the matrix viewed along the [100] zone axis, i.e., the $(001)_{Nd123}$ planes are imaged edge on. The image shows a curved area of the interface where interface steps can be observed. Interestingly, the height of the steps corresponds to one $(001)_{Nd123}$ lattice spacing. Taking into account that during thermal treatments performed below the peritectic temperature, the Nd422 phase is metastable, the observation of such steps at interface regions with small radius of curvature points to a dissolution process of the inclusion. Moreover, the Nd422 phase also forms a solid solution of the type $Nd_{4-2x}Ba_{2+2x}Cu_{2-x}O_{10-y}$, so that a redistribution of the concentration of Nd cations within a region close to the interface can be expected.

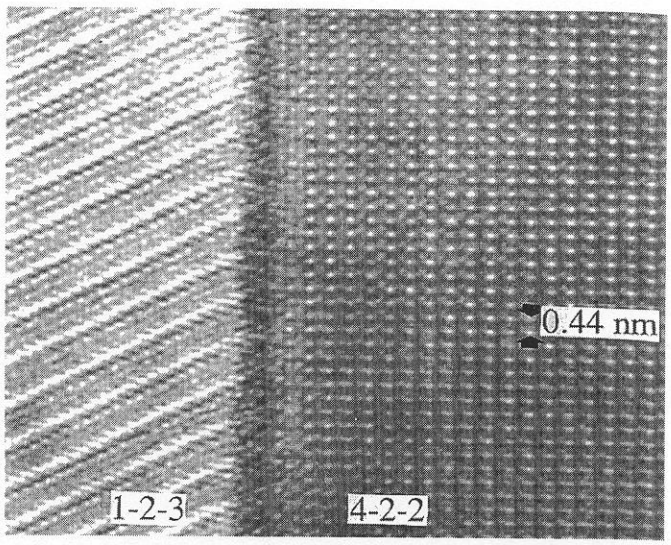

Fig. 1. *HRTEM image of a Nd422-Nd123 interface. The superconductor matrix is viewed along [001]. Some degree of lattice matching is achieved in this interface. Note the existence of a highly strained or amorphous layer at the interface.*

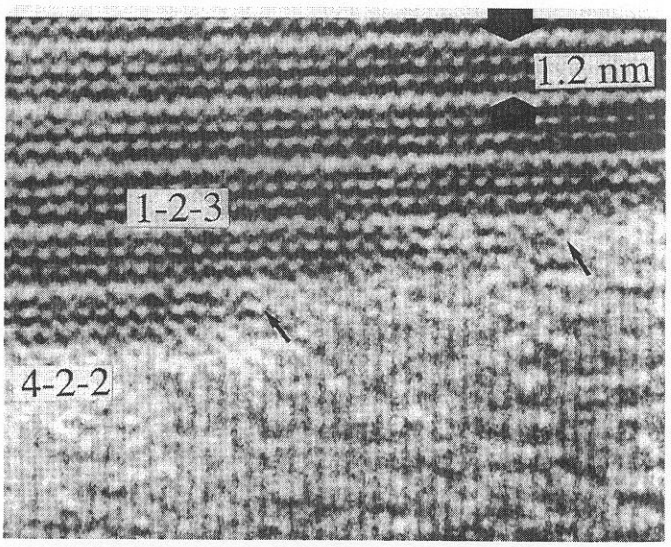

Fig. 2. *HRTEM image of a Nd422-Nd123 interface. The superconductor matrix is viewed along [001]. Note the formation of interface steps with height equal to one (001) lattice spacing of the Nd123 superconductor.*

The above microstructural observations point to a distinctive behaviour of Nd422-Nd123 interfaces compared with Y211-Y123 ones which could be at the origin of the observed difference of the $J_c(T)$ behaviour. Further characterisation of the Nd422-Nd123 interface microstructures will need high spatial resolution analytical techniques in order to determine the extent of compositional inhomogeneities associated with the observed defects.

3. DISLOCATIONS AND STACKING FAULT CONFIGURATIONS IN RE123 MATERIALS

Dislocation lines are line defects first proposed as pinning centres in classic superconductors (18). The effective area of a dislocation, i.e., the region where the material is not superconductor or the superconducting order parameter is depressed, may be divided into two parts: First, the core of radius ~ 1 to 5 times the Burgers vector (19), i.e., in the range 0.4 to 2 nm where the superconducting order parameter is suppressed due to loss of stoichiometry and crystallographic order. HRTEM images coupled with energy dispersive analysis of edge dislocations viewed end-on in a Y123 thin film, indicated a core radius of approximately 2 nm and a core composition enriched in copper (20). Secondly, each line has an associated long range strain field which varies as $1/r$ with distance r from the core (19). Therefore, if strains above 1% actually decrease the superconducting order parameter (21), the effective region is enlarged to a cylindrical area a few nanometers thick surrounding the core of the dislocation.

It appears that dislocations are very anisotropic pinning centres. Therefore relevant aspects of dislocations to the optimisation of the critical currents are the evaluation of their stable configurations and design of suitable processing techniques for controlling their density and orientation.

3.1. Dislocations

The stable dislocation configurations in Y123 have been theoretically studied using elastic anisotropy (22). These studies and TEM observations (23) reveal that dislocations in Y123 are confined to the basal plane of the crystal structure (001) and have Burgers vectors [100], [010] and <110>. For [100] and [010] dislocations, the most stable configuration is obtained when they are in edge orientation. On the other hand, <110> dislocations tend to adopt a screw orientation and can result from the reaction: [100]+[010]→[110]. Therefore, the most stable glide systems found in Y123 are [100](001), [010](001) and <110>(001). In order to obtain dislocation lines out of the (001) plane, climb mechanisms at sufficiently high temperatures, or specific deformation techniques to activate glide on different planes, are necessary. For instance, subgrain boundaries built up by dislocations with line directions close [001] are frequently found. On the other hand, the additional <110>{110}, [100](010) and [010](100) glide systems have been activated by shock compression (24).

In contrast with Y123 recent TEM studies indicate that the [100](010) and [010](100) glide systems, in addition to those present in Y123, are active in non-deformed Nd123 (25).

3.2. Stacking faults

In Y123 materials, stacking faults (SFs) with displacement vector $^1/_6$ <301> result either from the dissociation of a b=<100> or b=<110> (b is the Burgers vector) dislocation in $^1/_6$<301> partials (26), or from nucleation of a $^1/_6$<301> faulted loop at grain boundaries or inclusion-matrix interfaces (15,27). Such displacement vectors are consistent with the insertion of an extra CuO_x layer parallel to (001) between the two consecutive Ba sites of the crystal structure, giving rise to the formation of a double oxygen chain layer similar to that found in the Y124 compound (28). An alternative mechanism for the generation of SFs in melt textured Y123 has been proposed for samples solidified by a continuous zone melting process using a precursor mixture of sintered Y211, $BaCuO_2$ and CuO powders (29). Those authors argued that SFs could result from incomplete diffusion leading to the appearance of extra atomic planes in the Y123 phase. SFs formed by the second mechanism dominate in size and number in the final microstructure of melt processed Y123. On the other hand, SFs generated by the former mechanism, though being occasionally observed in as-solidified-oxygenated materials, are smaller and mostly generated by plastic deformation.

The formation of such double chain CuO_x layers is related to a local phase transformation (26,30) leading to a local 124 structure having a lower T_c than the 123 compound. In consequence, the size of such defects is not governed by the elastic interaction between dissociated segments but is determined by the thermodynamic stability and growth kinetics of the inserted CuO_x platelet (26). Interestingly, a model was proposed from Monte Carlo simulations, which satisfactorily predicts the nucleation of progressively CuO enriched local configurations upon increasing the CuO chemical potential (30). In Y123, when the SF is nucleated in a dislocation core (26) the feeding mechanism for the expansion of the extra layer is limited by pipe diffusion and after the conventional oxygenation treatment at 450°C their size is of about several nanometers. On the other hand, $^1/_6$<301> faulted loops nucleated at grain boundaries or at the interfaces of normal inclusions may achieve lengths up to a few microns (31) because such interfaces provide easy diffusion paths for copper and oxygen. Such faulted loops propagate by a non-stoichiometric partial dislocation climb mechanism, preferentially along the direction of the in-plane shear component of their Burgers vector, i.e., [100] or [010]. Such a preferred direction coupled with relatively high propagation rates leads to a «dendritic» or «finger-like» shape of the final configuration (Fig. 3).

As found Y123 materials, TEM characterisations of the microstructure in Nd123 have revealed that SFs have the same displacement vector thus suggesting that in this material they consist also of a double CuO_x layer (25). However the observed configurations display particular features. Fig. 4 is a bright field micrograph of a directionally solidified Nd123 sample showing narrow dark planar defects elongated in the [100] and [010] directions which correspond to $^1/_6$<301> SFs. Diffraction contrast analysis of the arrowed configuration indicated that such elongated defects are associated with the dissociation of a [110] dislocation according to the reaction

$$[110] \rightarrow {}^1/_2\,[110] + {}^1/_6[301] + {}^1/_6[03\bar{1}].$$

The dissociation leaves two SFs $^1/_6$ [301] and $^1/_6[03\bar{1}]$, separated by the $^1/_2$ [110] partial dislocation which exchanges the Burgers vectors of the dissociated segments along the [100] and [010] directions (25). The shape of the configuration suggests that the SFs have expanded rapidly in the direction of the in-plane component of their bounding partial dislocation in a similar way as that found in the SFs nucleated at interfaces in Y123, indicating that pipe diffusion along the dislocation cores is faster in Nd123 than in Y123.

One interesting aspect of the behaviour of SFs in melt textured Y123, in that their formation is sensitive to the thermal treatment of the samples. It has been reported that they can be annealed out by heating the sample in the temperature range 800-900°C (29,32), i.e., above the orthorhombic to tetragonal transition temperature (~600°C in air). Further insight into the stability range and kinetics of the local transformation leading to the nucleation of SFs has recently been provided by *in situ*

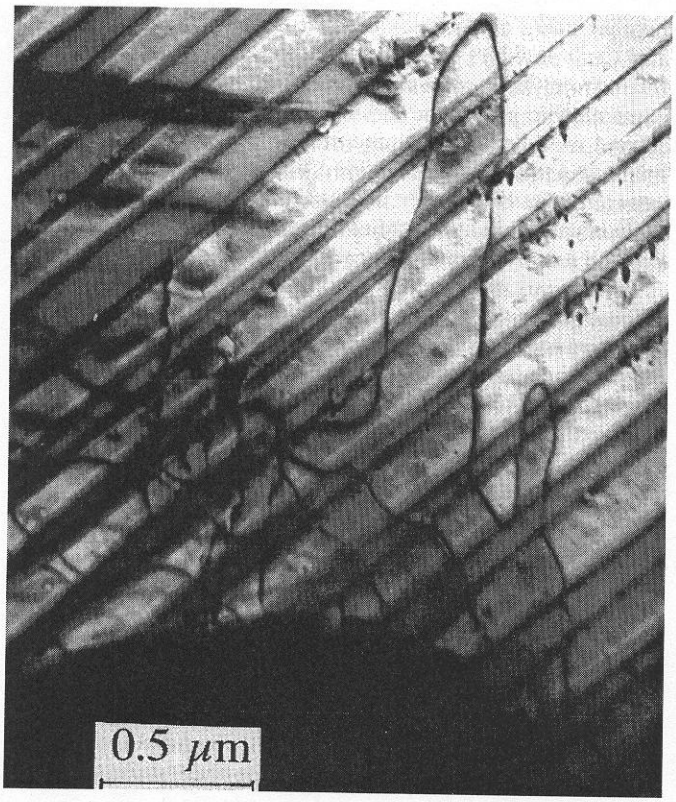

Fig. 3. *Bright field TEM micrograph showing large $^1/_6$ <301> faulted loops nucleated from a non-reacted inclusion interface during the oxygenation process at 450°C.*

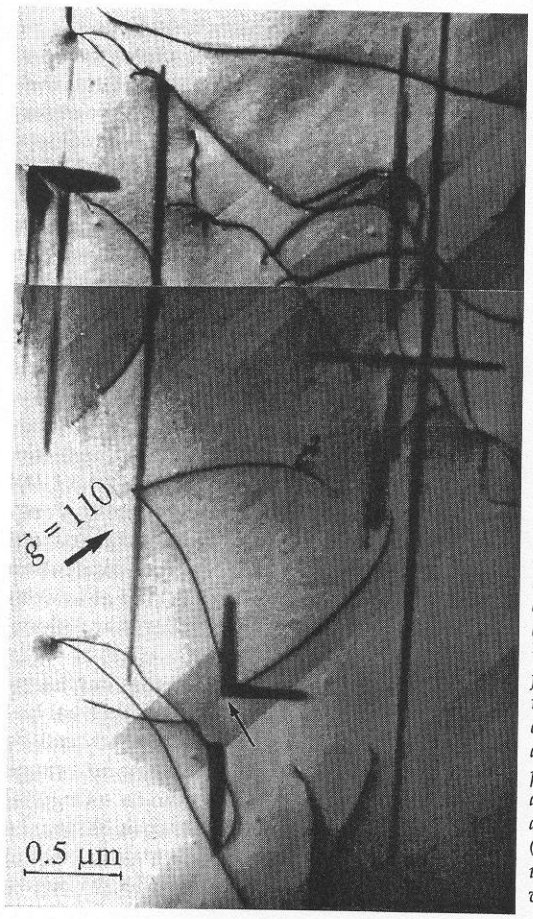

Fig. 4. *Bright field TEM micrograph showing different dislocation configurations in directionally solidified Nd123. Long and narrow dark defects are $^1/_6$ <301> faulted loops nucleated at a dislocation core and further propagated along [100] and [010] (Vilalta, unpublished work [25]).*

monitoring the dissolution process of $^1/_6$ <301> faulted loops nucleated at a Y211-Y123 interface in the TEM (33). This study indicated that the dissolution process is activated at the onset of the orthorhombic-to-tetragonal phase transition, thus evidencing the instability of such defects in the deoxygenated Y123 matrix, in agreement with the previous computer simulation results and TEM examinations of the microstructure of non-oxygenated as-solidified samples. From the processing point of view, the relevance of such studies lies in the fact that they indicate that these defects are unstable during solidification, and therefore, their size and density could be controlled by carefully adjusting the oxygenation parameters.

As a result of the strong sensitivity of SFs to the oxygenation conditions, the sample oxygenation step performed at temperatures around 450°C introduces important modifications of the microstructure and superconducting properties which have been characterised in Y123 materials (31,34). These results indicate that when the oxygenation time extents more than an optimal value, a strong ageing of the microstructure and irreversibility line occurs. The most prominent consequence is the development of large (up to a few microns) $^1/_6$ <301> faulted loops originating from easy diffusion paths like grain boundaries and Y211-Y123 interfaces by the mechanism outlined in the preceding section. In addition, preferential matrix decomposition at the SFs has been observed which ultimately lead to the formation of microcracks. A similar behaviour has been reported for ozone treated samples (35). From the microstructural modifications described above, it appears that an over-oxygenation of the samples results in a dramatic increase of planar defects lying on the (001) planes, namely SFs and microcracks, where the superconducting order parameter is depressed or even suppressed. When the samples are submitted to a magnetic field parallel to the [001] direction, the flux lines are cut by such planar defects thus increasing their thermal activation resulting in a shift of the irreversibility line towards lower temperatures and magnetic fields (31,34).

3.3. Deformation processing

The motivation for plastic deformation experiments in superconducting materials is to increase the number of dislocations acting as flux pinning centres and to explore the possibility to activate glide in planes other than (001). Deformation techniques used so far in melt textured materials include shock compression (24), hot isostatic pressing (36,37), high temperature uniaxial compression (36-40) and room temperature uniaxial compression (41).

Because of the brittleness of the Y123 material, in order to achieve significant plasticity, temperatures around 900°C are needed. It was reported that even at such elevated temperatures, plastic deformation is less than 8% of total strain (38,42). At high temperatures, moreover, we are faced with different factors influencing the final microstructure: First, point defect diffusion in addition to strain effects, presumably plays an important role (43); second, TEM studies of the as-deformed microstructure, i.e., before oxygenation, indicated that deformation is produced in the deoxygenated phase, (38). As a result, the samples need to be re-oxygenated after deformation in order to restore the superconducting orthorhombic phase. This oxygen anneal inevitably causes severe modifications of the as-deformed microstructure (38).

Early microstructural characterisations of plastically deformed 123 melt textured materials (37) revealed a dislocation density of $2x10^{10}$ cm^{-2}, one order of magnitude higher than in

non-deformed samples. Such an increase of the dislocation density could be nicely correlated with a concomitant increase of J_c (36, 44, 45). Most of dislocations were found to have Burgers vectors [100] and [010], forming pile-ups along the [100] and [010] directions. However, subsequent investigations suggested that the deformation mechanism could depend on the sample characteristics. Actually the samples reported on ref. (37,36) displayed a low initial value of J_c at 77 K (J_c(H=0)~$3x10^4$ A/cm^2) and after the plastic deformation it was increased by a factor of ~2, i.e. still lower than the highest J_c value (J_c~10^5 A/cm^2) reported in Y123 composites. Inductive J_c measurements have been conducted in high temperature uniaxially deformed samples displaying initially high J_c (around 10^5 A/cm^2 in self field at 77K) and a fine dispersion of Y211 precipitates (39% in weight). Surprisingly, after deformation and the corresponding reoxygenation annealing at 450°C, the superconducting behaviour was severely degraded (39,40). The observed discrepancies between the behaviour of different samples, indeed suggest that plastic deformation cannot be used as an universal technique but is largely influenced by the original microstructure of the material.

Since the final scope of such experiments is to increase the density of dislocations acting as flux pinning centres, it appears that important drawbacks of hot plastic deformation processing of high J_c Y123 materials having a high concentration of Y211 inclusions, are (38,39): First, the primary creep stage where new dislocations are introduced (46) is very small in melt textured Y123 materials. Secondly, the oxygenation process causes a dramatic modification of the as-deformed microstructure, including dislocation annihilation and the formation of a high density of SFs and microcracks which lead to a downward shift of the irreversibility line in the H//[001] configuration. In order to overcome these drawbacks new strategies such as deformation at room temperature under a confining pressure (41) or high temperature deformation under an oxydising atmosphere are currently investigated in different laboratories. Regarding Nd123, no deformation experiments have been yet reported, however this compound offers interesting opportunities for the creation of dislocation lines perpendicular to the CuO_x layers.

4. SUBGRAIN BOUNDARIES

Despite the tremendous effort conducted towards improving J_c in melt textured RE123 materials, the highest values achieved up to date lie about a factor of ten below those achieved in irradiated single crystals ($1.3x10^7$ A/cm^2, 5K, zero field (47)) or optimized thin films ($1.6x10^7$ A/cm^2, 5K, zero field (48)). Looking at the microstructure, subgrain boundaries appear as the most likely current limiting defects in melt processed materials.

During sample cooling from the solidification temperature and during the oxygenation step, when dislocation climb is possible, gliding dislocations are trapped by non-superconducting inclusions and further rearranged on dislocation walls preferentially parallel to the {100} and {110} planes (49). The mosaic spread arising from such dislocation rearrangement is demonstrated in the (006) rocking curve shown in Fig. 5, obtained over a few mm^2 area in a single domain region. Interestingly, the rocking curve presents a total misorientation spread over an angular range of ~10°. The analysis of the rocking curve (49) led to the interpretation that the mosaic structure is developed in two length scales, responsible for the

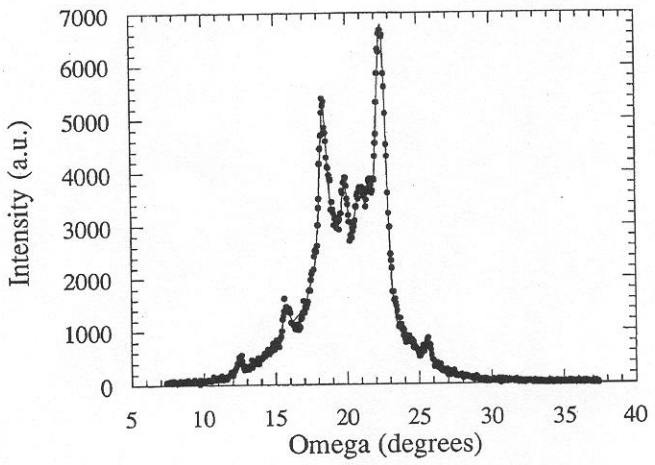

Fig. 5. *X-ray diffraction rocking curve of the (006) reflection measured over an area of ~5 mm^2*

continuous background and the sharp peaks. This interpretation is indeed consistent with TEM observations (49) revealing a high density of «very small» angle ($\theta < 1°$) subgrain boundaries interconnecting Y211 particles. In composites having a high concentration of small (<1μm) 211 precipitates, such subgrain boundaries are spaced by ~1-2 μm, and are likely responsible for the continuous gaussian background of the rocking curve. On a larger scale, subgrain boundaries involving larger misorientations occur, which are correlated with the sharp peaks. TEM observations revealed that such subgrain boundaries are not regularly spaced and do not present a trivial correspondence with the Y211 precipitate size and density.

It appears that even when solidification conditions have been optimized such as to obtain a single flat growth front, the resulting single domain sample is still plagued by subgrain boundaries. The density of subgrain boundaries increases with the density of Y211 particles. Therefore, understanding of the processes limiting critical currents in melt textured RE123 materials will need a detailed characterisation of subgrain boundary local microstructure.

First evidence for a correlation between grain boundary (GB) microstructure and electromagnetic behaviour came from the Dimos et al. (50) plots displaying the critical current at the GB [J_c(GB)] *versus* misorientation angle θ. Such studies were performed on artificial bicrystal films and the GB were mainly symmetrical θ[001] and symmetrical θ[100] tilts. The plot clearly identifies two regimes: For θ values in the range ~5° to ~10°, voltage-current behaviour reflected the existence of weak electromagnetic coupling across the boundary; and for θ>10° J_c(GB) is approximately independent of θ, with a small ratio of J_c(GB) to J_c in the grain ~10^{-2}. Taking into account that such symmetrical tilt GBs are built by one set of equidistant dislocations parallel to the rotation axis, spaced by approximately b/θ the plateau regime which appeared for misorientations larger than 10° could be nicely correlated with the misorientation range where the boundary dislocations would overlap. In the low angle regime (<10°) the shape of the J_c(GB)(θ) dependence was better described taking into account the elastic-strain field around GB dislocations (21). Such observations indeed point to a correlation between microstructure, namely GB dislocations (GBDs) and associated strain fields, and electromagnetic properties, the controlling factor being the density in the GBD network. Such observations are in fact

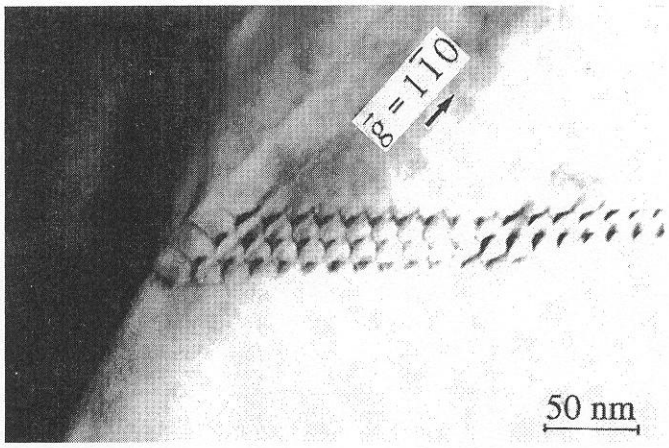

Fig. 6. *Bright field TEM micrograph showing a honeycomb-like dislocation network. The rotation axis is [001] and misorientation angle varies through the boundary with values smaller or equal to 1 degree (Vilalta, unpublished work [25]).*

consistent with proposed GB models which point to a subdivision of the GB into channels with different electrical properties (51). Evidence for channel conduction in 3°-20°[001] tilt bicrystal films has indeed been recently reported (52). However it must be taken into account that experiments correspond to a particular boundary geometry. The geometry of the GBD network is determined by the stable Burgers vectors of the dislocations, the relation between boundary plane and rotation axis orientation, and the rotation angle which determines the dislocation density for a given configuration. In fact, a few works report on more than one set of GBDs (53, 49,54). An example of a honeycomb like network composed of [100], [010] and [110] dislocations in a boundary with a misorientation angle of approximately one degree, is shown in Fig. 6 (55). Therefore, when dealing with arbitrary boundary parameters, use of Dimos plots to estimate the influence on J_c from rotation angle may be unrealistic. A more realistic reading of such plots could be done by substituting the rotation angle, θ, by the corresponding dislocation density given in that case by θ/b. Unfortunately, the determination of the dislocation line density in an arbitrary GB is complicated and no estimations have yet been reported.

Another characteristic of GBs in Y123 materials is the strong tendency to faceting of the boundary plane. GBs in Y123 are preferentially faceted along the {100} and {110} planes. As a consequence, deviations from the preferred planes are often accommodated by the formation of an stepped interface (49). Faceting of the boundary plane may have implications on the coupling strength across the GB. First, an accurate TEM study revealed extensive strain contrast was found associated with the intersections of several facets in a ~6°[001] tilt flux grown bicrystal (56). The extent and strength of this contrast was also found to be noticeably larger than that associated with individual GBDs. As a result, the fraction of strained material within the boundary where the superconducting order parameter can be depressed, is increased at facet junctions thus narrowing the width of the superconducting channels. On the other hand, in the same GB, it was found that the dislocation spacing near the centre of some facets is smaller than near the facet junctions. Such inhomogeneous GBDs distributions are likely to result from finite size effects of individual facets (56). As suggested by Field et al (57), sets of unevenly spaced dislocations would explain the observed residual currents in GBs with misorientation angles for which an infinite set of uniformly spaced GBDs would overlap causing weak link behaviour.

5. CONCLUSION

Among the various defects present in melt textured RE123 materials, non-superconductor/superconductor sharp interfaces have been identified as a dominant flux pinning centre. While such interfaces are provided by Y211 non-reacted inclusions in Y123, recent experimental results point to a reduced efficiency of Nd422 interfaces in Nd123.

Current processing techniques do not allow to modify the dislocation substructure in controlled way. High temperature deformation suffers from two important drawbacks. First, the low plasticity (up to ~4% of total strain) achieved in high temperature creep experiments, and the complex diffusive processes governing the secondary creep stage do not allow a substantial increase of the dislocation density. Secondly, the post deformation oxygenation step carried out at 450°C generates a high concentration of large planar defects parallel to (001) which enhance the thermal activation of flux line motion resulting in an undesirable shift of the irreversibility line to lower fields and temperatures. It appears that dislocation control in such ceramics needs new strategies avoiding the oxygenation step. Considering the high anisotropy of the dislocation configurations, the recent identification of [100](010) and [010](100) glide systems in Nd123 offers new opportunities in the design of plastic deformation experiments.

Finally, subgrain boundaries appear as an intrinsic limitation for higher J_c values. The observation of relatively dense dislocation networks in subgrain boundaries involving misorientation angles as small as about one degree, together with their high concentration which correlates with the density of non-superconducting inclusions, situates the observed narrow mosaic substructure at the origin of the gap separating J_c values achieved in melt textured materials and thin films or single crystals.

ACKNOWLEDGEMENTS

The author acknowledges his colleagues N. Vilalta, X. Obradors, B. Martínez, J. Rabier, and J. Fontcuberta for illuminating discussions. Special thanks to N. Vilalta for sharing some unpublished material. ◆

REFERENCES

1. P. McGuinn, in «High Temperature Superconducting Materials Science and Engineering», edited by Donglu Shi (Elsevier Science Ltd. 1995). Chapter 8, pp. 345-382.
2. S. Piñol, F. Sandiumenge, B. Martínez, V. Gomis, J. Fontcuberta, X. Obradors, E. Snoeck, and Ch. Roucau, «Enhanced critical currents by CeO_2 additions in directionally solidified $YBa_2Cu_3O_{7-x}$», Appl. Phys. Lett. 65, 1448-1450 (1994).
3. L. Civale, A. D. Marwick, T. K. Washington, M. A. Kirk, J. R. Thompson, L. Krusin-Elbaum, Y. Sun, J. R. Clem, and F. Holtzberg, «Vortex confinement by columnar defects in $YBa_2Cu_3O_{7-x}$ crystals: enhanced pinning at high fields and temperatures» Phys. Rev. Lett. 67, 648-652 (1991).
4. L. Krusin-Elbaum, J. R. Thompson, R. Wheeler, A. D. Marwick, C. Li, S. Patel, D. T. Shaw, P. Lisowski and J. Ullmann, «Enhancement of persistent currents in $Bi_2Sr_2CaCu_2O_8$ tapes with splayed columnar defects induced

with 0.8 GeV protons», Appl. Phys. Lett. 64, 3331-3334 (1994).
5. P. Yang and C. M. Lieber, «Nanorod-superconductor composites: A pathway to materials with high critical current densities», Science 273, 1836-1840 (1996).
6. F. Sandiumenge, B. Martínez and X. Obradors, «Tailoring of microstructure and critical currents in directionally solidified $YBa_2Cu_3O_{7-x}$», Supercond. Sci. Technol. 10 (1997) 10, A93-A119 (1997).
7. F. Sandiumenge, S. Piñol, X. Obradors, E. Snoeck, and Ch. Roucau, «Microstructure of high critical current directionally solidified $YBa_2Cu_3O_7$-Y_2BaCuO_5 composites» Phys. Rev. B 50, 7032-7045 (1994).
8. M. Murakami, H. Fujimoto, S. Gotoh, K. Yamaguchi, N. Koshizuka and S. Tanaka, «Flux pinning due to nonsuperconducting particles in melt processed YBaCuO superconductors», Physica C 185-189, 321-324 (1991).
9. B. Martínez, X. Obradors, A. Gou, V. Gomis, S. Piñol, J. Fontcuberta and H. Van Tol, «Critical currents and pinning mechanisms in directionally solidified $YBa_2Cu_3O_7$-Y_2BaCuO_5 composites», Phys. Rev. B-53, 2797-2810 (1996).
10. T. Izumi, Y. Nakamura and Y. Shiohara, «Doping effects on coarsening of Y_2BaCuO_5 phase in liquid», J. Mater. Res. 8, 1240-1246 (1993).
11. L. Durand and J. L. Pastol, «Dy_2BaCuO_5 distribution in melt textured $DyBa_2Cu_3O_y$ superconductors prepared by the horizontal Bridgman method», Mater. Lett., 19, 291-296 (1994).
12. M. Murakami (1992) «Melt processed high-temperature superconductors» ed M. Murakami (Singapore: World Scientific) ch. 3, pp. 21-44.
13. N. Vilalta, F. Sandiumenge, S. Piñol, and X. Obradors, «Precipitate size refinement by CeO_2 and Y_2BaCuO_5 additions in directionally solidified $YBa_2Cu_3O_7$», J. Mater. Res. 12, 38-46 (1997).
14. C-J. Kim, K-B. Kim, D-Y. Won, H-C Moon, D-S. Suhr, S. H. Lai, and P. J. McGuinn, «Formation of $BaCeO_3$ and its influence on microstructure of sintered/melt textured Y-Ba-Cu-O oxides with CeO_2 addition», J. Mater. Res. 9, 1952-1960 (1994).
15. K. Yamaguchi, M. Murakami, H. Fujimoto, S. Gotoh, T. Oyama, Y. Shiohara, N. Koshizuka, ans S. Tanaka, «Microstructures of melt powder melt growth processed YBaCuO», J. Mater. Res. 6, 1404-1407 (1991).
16. R. Yu, F. Sandiumenge, B. Martínez, N. Vilalta and X. Obradors, «Interface pinning in high T_c -high J_c $Nd_{1-x}Ba_{2-x}Cu_3O_y$ directionally solidified in air», Appl. Phys. Lett. (1997) in press.
17. F. Sandiumenge and N. Vilalta (1997), unpublished results.
18. A. M. Campbell and J. E. Evetts, «Flux vortices and transport currents in type II superconductors», Adv. Phys. 21, 199-428 (1972).
19. J.P. Hirth and J. Lothe, "Theory of dislocations" (John Wiley & Sons, N.Y., 1982).
20. Y. Gao, K. L. Merkle, G. Bai, H. L. M. Chang and D. J. Lam, «Structure and composition of grain boundary dislocations cores and stacking faults in MOCVD-grown $YBa_2Cu_3O_7$ films», Physica C, 174, 1-9 (1991).
21. M. F. Chislom and S. J. Pennycook, «Structural origin of reduced currents at $YBa_2Cu_3O_{7-x}$ grain boundaries» , Nature 351, 47-50 (1991).
22. J. Rabier, «Stable dislocation configurations in $YBa_2Cu_3O_7$» in «Plastic deformation of ceramic materials», Plenum Press; R. C. Bradt, C. A. Brookes, J. L. Routbort editors; 1995, pp. 403-408.
23. J. Rabier and M. F. Denanot, «Plastic deformation of $YBa_2Cu_3O_{7-x}$ and related defects», Rev. Phys. Appl. 25, 55-63 (1990).
24. M. Verwerft, D. K. Dijken, J. Th. M. De Hosson, and A. C. Van Der Steen, «Different types of dislocations in $YBa_2Cu_3O_{7-x}$» , Phys. Rev. B, 50 3271-3281 (1994).
25. N. Vilalta (1997), unpublished results.
26. J. Rabier, P. D. Tall, and M. F. Denanot, «On the dissociation of dislocations in $YBa_2Cu_3O_{7-x}$», Philos. Mag. A 67, 1021-1029 (1993).
27. H. Gu, C. Colliex, S. Senoussi, C. Aguillon-Levillain, and P. Manuel, «Generation and dissociation of dislocations in $YBa_2Cu_3O_{7-x}$ single crystals and deformed oriented powders» Philos. Mag. A 68, 19-29 (1993).
28. H. W. Zandbergen, R. Gronsky, K. Wang, and G. Thomas, « Structure of $(CuO)_2$ double layers in superconducting $YBa_2Cu_3O_7$», Nature 331, 596-599 (1988).
29. P. X. Zhang, L. Zhou, P. Ji, W. M. Bian, X. Z. Wu, and Z. H. Lai, «The effect of annealing on stacking faults and J_c values of PMP processed YBaCuO», Supercond. Sci. Technol. 8, 15-19 (1995)
30. M. Fendorf, C. P. Burmester, L. T. Wille, and R. Gronsky, «Copper-oxygen intercalation and related phase transformations in YBaCuO», Appl. Phys. Lett. 57, 2481-2483 (1990).
31. F. Sandiumenge, N. Vilalta, S. Piñol, B. Martínez, and X. Obradors, «Aging of the microstructure of melt textured $YBa_2Cu_3O_7$-Y_2BaCuO_5 composites and implications on their superconducting properties», Phys. Rev. B 51, 6645-6654 (1995).
32. Y. H. Zhang, V. Selvamanickam, D. F. Lee, and K. Salama, «Evidence of enhanced flux pinning by dislocations in deformed textured $YBa_2Cu_3O_{7-x}$ superconductors», Jpn. J. Appl. Phys. 33, 3419-3425 (1994).
33. F. Sandiumenge, N. Vilalta, Y. Maniette, and X. Obradors, «Stability and evolution of stacking faults in melt textured $YBa_2Cu_3O_{7-x}$», Appl. Phys. Lett. 70, 2192-2194 (1997).
34. B. Martínez, F. Sandiumenge, S. Piñol, N. Vilalta, J. Fontcuberta, and X. Obradors, «Aging of critical currents and irreversibility line in melt textured $YBa_2Cu_3O_{7-x}$», Appl. Phys. Lett. 66, 772-774 (1995).
35. Y. Zhu, R. L. Sabatini, Y. L. Wang, and M. Suenaga, «Effect of ozone oxygenation of $YBa_2Cu_3O_{7-x}$ thin crystals», J. Appl. Phys. 73, 3407-3412 (1993).
36. V. Selvamanickam, M. Mironova, S. Son, and K. Salama, «Flux pinning by dislocations in deformed melt textured $YBa_2Cu_3O_{7-x}$ superconductor» Physica C 208, 238-244 (1993).
37. M. Mironova, V. Selvamanickam, D. F. Lee, and K. Salama, «TEM studies of dislocations in defromed melt textured $YBa_2Cu_3O_{7-x}$ superconductor», J. Mater. Res. 8, 2767-2773 (1993).
38. N. Vilalta, F. Sandiumenge, J. Rabier, M. F. Denanot and X. Obradors, «Evolution of the microstructure during high-temperature creep and oxygenation in directionally solidified $YBa_2Cu_3O_{7-x}$ « Phil. Mag. A (1997) (in press).
39. N. Vilalta, F. Sandiumenge, E. Rodríguez, B. Martínez, S. Piñol, X. Obradors, and J. Rabier, «Microstructure, irreversibility line and flux dynamics in plastically deformed directionally solidified $YBa_2Cu_3O_{7-x}$ «, Philos. Mag. B, 75, 431-441 (1997).
40. B. Martínez, F. Sandiumenge, N. Vilalta, S. Piñol, X. Obradors, and J. Rabier, «Plastic deformation in high critical current melt textured $YBa_2Cu_3O_{7-x}$ « J. Appl. Phys. 80, 5515-5518 (1996).
41. L. Richard, «Défauts, plasticité et propriétés physiques induites des supraconducteurs à haute température critique: $YBa_2Cu_3O_{7-x}$, « Thèse pour l'obtention du grade de docteur, Universite de Poitiers (1997).
42. D. Rodgers, K. White, V. Selvamanickam, A. McGuire, and K. Salama, «Plastic deformation of melt textured $YBa_2Cu_3O_{7-x}$ superconductor at elevated temperatures», Supercond. Sci. Technol., 5, 640-646 (1992).
43. T. Bretheau, J. Castaing, J. Rabier, and P. Veyssière, «Dislocation motion and high temperature plasticity of binary and ternary oxides», Adv. Phys. 28, 835-1014 (1979).
44. V. Selvamanickam, M. Mironova, and K. Salama, «Enhancement critical current density in $YBa_2Cu_3O_{7-x}$ superconductors by mechanical deformation», J. Mater. Res., 8, 249-255 (1993).
45. Y. H. Zhang, V. Selvamanickam, D. F. Lee, and K. Salama, «Evidence of enhanced flux pinning by dislocations in deformed textured $YBa_2Cu_3O_{7-x}$ superconductors», Jpn. J. Appl. Phys. 33, 3419-3424 (1994).
46. J. P. Poirier , «Creep of Crystals (High temperature processes in metals, ceramics and minerals)» , Cambridge University press, (London, 1985).
47. R. Griessen, Wen Hai-hu, A.J.J. Van Dalen, B. Dam, J. Rector, H.G. Schnack, S. Libbrecht, E. Osquiguil and Y. Bruynseraede, «Evidence for mean free path fluctuation induced pinning in $YBa_2Cu_3O_7$ and $YBa_2Cu_4O_8$ films» , Phys. Rev. Lett. 72, 1912-1915 (1994).
48. L. Civale, A. D. Marwick, T. K. Washington, M. A. Kirk, J. R. Thompson, L. Krusin-Elbaum, Y. Sun, J. R. Clem, and F. Holtzberg, «Vortex confinement by columnar defects in $YBa_2Cu_3O_{7-x}$ crystals: enhanced pinning at high fields and temperatures», Phys. Rev. Lett. 67, 648-6451 (1991).
49. F. Sandiumenge, N. Vilalta, X. Obradors, S. Piñol, J. Bassas, and Y. Maniette, «Polygonization of directionally solidified high critical current $YBa_2Cu_3O_{7-x}$ «, J. Appl. Phys. 79, 8847-8849 (1996).
50. D. Dimos, P. Chaudhari, J. Mannhart, and F. K. LeGoues, «Orientation dependence of grain boundary critical currents in $YBa_2Cu_3O_{7-x}$ bicrystals» , Phys. Rev. Lett. 61, 219-223 (1988).
51. E. Sarnelli, P. Chaudhari, and J. Lacey, «Residual critical current in high-T_c grain boundary junctions», Appl. Phys. Lett. 62, 777-779 (1993).
52. N. F. Heinig, R. D. Redwing, I.-F. Tsu, A. Gurevich, J. E. Nordman, S. E. Babcock and D. C. Larbalestier, «Evidence for channel conduction in low misorientation angle [001] $YBa_2Cu_3O_{7-x}$ bicrystal films» , Appl. Phys. Lett. 69, 577-579 (1996).
53. Y. Zhu, H. Zhang, H. Wang, and M. Suenaga, «Grain boundary in textured $YBa_2Cu_3O_{7-x}$ superconductor», J. Mater. Res. 6, 2507-2517 (1991).
54. Y. Zhu, «Studies of the crystallography of arbitrary grain boundaries by O-lattice construction: application to bulk $YBa_2Cu_3O_{7-x}$», Phil. Mag. A 69, 717-725 (1994).
55. F. Sandiumenge (1997), unpublished results.
56. I.-F. Tsu, S. E. Babcock and D. L. Kaiser, «Faceting, dislocation network structure, and various scales of heterogeneity in a $YBa_2Cu_3O_{7-x}$ low angle [001] tilt boundary» , J. Mater. Res. 11, 1383-1394 (1996).
57. M. Field, D. C. Larbalestier, A. Parikh and K. Salama, «Critical current properties and the nature of the electromagnetic coupling in melt-textured $YBa_2Cu_3O_{7-x}$ bicrystals of general misorientation», 280, 221-233 (1997).